Study of the effective point of measurement for ion chambers in electron beams by Monte Carlo simulation

L. L. W. Wang[a)] and D. W. O. Rogers[b)]
Ottawa Carleton Institute of Physics, Carleton University Campus, Ottawa K1S 5B6, Canada

(Received 16 December 2008; revised 28 March 2009; accepted for publication 29 March 2009; published 5 May 2009)

In current dosimetry protocols for electron beams, for plane-parallel chambers, the effective point of measurement is at the front face of the cavity, and, for cylindrical chambers, it is at a point shifted $0.5r$ upstream from the cavity center. In this study, Monte Carlo simulations are employed to study the issue of effective point of measurement for both plane-parallel chambers and cylindrical thimble chambers in electron beams. It is found that there are two ways of determining the position of the effective point of measurement: One is to match the calculated depth-ionization curve obtained from a modeled chamber to a calculated depth-dose curve; the other is to match the electron fluence spectrum in the chamber cavity to that in the phantom. For plane-parallel chambers, the effective point of measurement determined by the first method is generally not at the front face of the chamber cavity, which is obtained by the second method, but shifted downstream toward the cavity center by an amount that could be larger than one-half a millimeter. This should not be ignored when measuring depth-dose curves in electron beams. For cylindrical chambers, these two methods also give different positions of the effective point of measurement: The first gives a shift of $0.5r$, which is in agreement with measurements for high-energy beams and is the same as the value currently used in major dosimetry protocols; the latter gives a shift of $0.8r$, which is closer to the value predicted by a theoretical calculation assuming no-scatter conditions. The results also show that the shift of $0.8r$ is more appropriate if the cylindrical chamber is to be considered as a Spencer-Attix cavity. In electron beams, since the water/air stopping-power ratio changes with depth in a water phantom, the difference of the two shifts $(0.3r)$ will lead to an incorrect evaluation of the water/air stopping-power ratio at the point of measurement, thus resulting in a systematic error in determining the absorbed dose by cylindrical chambers. It is suggested that a shift of $0.8r$ be used for electron beam calibrations with cylindrical chambers and a shift of $0.4r$–$0.5r$ be used for depth-dose measurements.
[DOI: 10.1118/1.3121490]

Key words: effective point of measurement, ion chamber dosimetry, electron beams, dosimetry protocols, Monte Carlo, EGSnrc

I. INTRODUCTION

In the AAPM's TG-21 (Ref. 1) dosimetry protocol, the replacement correction factor P_{repl} is expressed as

$$P_{\mathrm{repl}} = P_{\mathrm{gr}} P_{\mathrm{fl}}, \tag{1}$$

where P_{gr} is the gradient correction and P_{fl} is the fluence correction (corresponding to the displacement perturbation p_{dis} and the fluence perturbation p_{cav}, respectively, in the IAEA's notation). For photon beams, P_{fl} is taken as 1 as transient charged particle equilibrium exists beyond d_{max}, so P_{repl} is just P_{gr}. For electron beams both P_{gr} and P_{fl} are nonunity and the perturbation effect is much more complicated. In fact, in electron beams, the shape of the electron fluence spectrum is continuously changing with depth. This is not a big issue for plane-parallel chambers as the front face of the cavity is taken as the point of measurement, i.e., the shape of the electron fluence spectrum in the cavity is very similar to that in the phantom at the point of measurement.[2] For cylindrical chambers with the central axis as the point of measurement, it does present a problem: The electron fluence spectrum in the cavity has a higher average energy than that in the phantom at the point of measurement since the electrons lose less energy in the cavity's air. This difference in the electron fluence spectrum results in values of P_{repl} significantly different from unity even at d_{max} for low-energy beams (e.g., ~0.96 for Farmer chambers in a 6 MeV beam) and huge correction factors in the dose fall-off region where the dose gradient is very large. This is why cylindrical chambers are not recommended for use in low-energy electron beams.[3,4] Instead of using depth-dependent gradient correction factors, use of an effective point of measurement (EPOM) is recommended for cylindrical chambers in electron beams. Current dosimetry protocols[3,4] shift the effective point of measurement upstream by $0.5r$ from the chamber center for a cylindrical chamber having a cavity radius r. This value of shift originates mainly from the experimental work of Johansson *et al.*[5] Although the AAPM's TG-51 protocol[3] explicitly uses a gradient correction factor P_{gr}, it is defined as the ratio of chamber reading at a depth $0.5r$ shifted downstream from the point of measurement to that at the point of measurement. Hence it is equivalent to the approach of a shift of effective point of measurement as done in IAEA's Code of Practice[4] if one ignores the difference of the other correction factors at these two depths.

Experimentally, the effective point of measurement of a cylindrical thimble chamber is determined by comparison of the percentage depth-dose (PDD) curves measured by both the cylindrical chamber and a plane-parallel chamber with its inner-front wall as the measuring point. The PDD curve measured by the cylindrical chamber is shifted upstream in order to match the curve obtained by the plane-parallel chamber on the assumption that the plane-parallel chamber has no shift. However, there is experimental evidence that the effective point of measurement for plane-parallel chambers in electron beams might not be at the front surface of the air cavity. Van der Plaetsen *et al.*[6] compared the measured d_{max} and R_{50} between a Markus chamber and a Roos chamber for a variety of electron beams and made a conclusion that the effective point of measurement for the Markus chamber should be shifted by 0.5 mm from the front face of the cavity toward the center of the cavity. Roos *et al.*[6] performed similar experiments and arrived at the same conclusion. In this study, Monte Carlo simulations using EGSnrc (Refs. 7 and 8) codes are employed to study the issue of effective point of measurement for both cylindrical chambers and plane-parallel chambers in electron beams. The electron fluence spectra in both the phantom and the chamber cavities are calculated and their change vs depth is studied. The Monte Carlo calculation methods employed have been compared to experimental measurements in a variety of situations regarding P_{repl} and found to be in good agreement with measured values.[2,9,10]

II. EFFECTIVE POINT OF MEASUREMENT

II.A. The EGSnrc Monte Carlo calculations

As depth-dose curves and depth-ionization curves for ion chambers can be calculated by Monte Carlo simulations, one may find the effective point of measurement computationally not only for cylindrical chambers but also for plane-parallel chambers. In this study, the depth-dose curves are calculated by the EGSnrc user-code DOSRZnrc,[11] and the water/air stopping-power ratio is calculated by the EGSnrc user-code SPRRZnrc (Ref. 11) using the standard $\Delta = 10$ keV cutoff used in dosimetric protocols. Kawrakow's C++-based EGSnrc user-code CAVITY (Ref. 12) is used in all the chamber depth-ionization calculations (i.e., the dose in the air cavity of the modeled chambers vs depth). We implemented the capability of calculating the electron fluence spectrum and the total electron fluence in the CAVITY code and it gives identical results to the widely used FLURZnrc (Ref. 11) user code when RZ geometries are modeled. Modeled chambers are put at various depths in a water phantom irradiated by phase-space sources of either a 6 or a 22 MeV electron beam. The phase-space files were generated from a BEAMnrc (Ref. 13) model for a 6 MeV Varian Clinac 2100C linac and a 22 MeV Elekta SL25 linac, both having a 100 cm source-surface distance and a 10×10 cm^2 field size. For all plane-parallel chamber calculations, the point of measurement is taken to be the front face of the air cavity and for all the cylindrical chamber calculations, the point of measurement is at the center of the air cavity. The electron and photon energy thresholds for production and tracking (AE, ECUT and AP, PCUT) are 521 keV (10 keV kinetic energy) and 10 keV, respectively, except in electron fluence spectrum calculations where the energy extends to 512 keV. For the electron fluence spectrum calculation, the thickness of the in-phantom scoring voxel is 0.2 mm.

II.B. Determining the EPOM from depth-ionization curves

According to the Spencer-Attix formalism,[14,15] the dose in water, D_{water}, is related to the dose in an ideal Spencer-Attix cavity, D^s_{air}, by

$$D_{water} = D^s_{air}\left(\frac{\bar{L}_\Delta}{\rho}\right)^{water}_{air}, \tag{2}$$

where $(\bar{L}_\Delta/\rho)^{water}_{air}$ is the Spencer-Attix water/air mean restricted mass collision stopping-power ratio with cutoff energy Δ. For a real chamber model, the dose in the air cavity, D_{air}, can be related to the dose in the ideal Spencer-Attix air cavity through a perturbation factor P,

$$D^s_{air} = D_{air}P. \tag{3}$$

The calculated depth-dose curves are converted to the fractional depth-ionization (FDI) curves for an ideal Spencer-Attix cavity (referred to as the ideal FDI) by dividing by $(\bar{L}_\Delta/\rho)^{water}_{air}$ at each depth. This results in D^s_{air} in Eq. (3), which is compared to the depth-ionization curves obtained by the modeled chamber calculation at depths, i.e., D_{air} in Eq. (3) (referred to as the chamber FDI). Both the FDI curves are normalized to 1.0 at their respective maximum ionizations. The matching of the two curves effectively minimizes the average value of the perturbation correction (i.e., $|1-P|$) at all depths. Figure 1 shows a comparison of the ideal and the chamber FDI curves thus obtained for (a) a 6 MeV and (b) a 22 MeV electron beam. The ideal FDI has a spatial resolution of 0.5 mm (1 mm) for the 6 MeV (22 MeV) electron beam and the chamber FDI has a spatial resolution of 1 mm (5 mm) for the respective electron beam. To determine the distance of shift needed to match the chamber FDI to the ideal FDI, the following procedure is followed: (1) A series of shift values, defined as negative if the shift is upstream to the source, is applied to all the depths of the chamber FDI curve; (2) for each shift s, the values on the chamber FDI curve are multiplied by a scaling factor α, which can be obtained by minimizing the root-mean-square (rms) difference between the two FDI curves. The scaling factor is necessary because normalization at the calculated maximum ionization gives undue importance to that single depth. The rms difference is calculated as

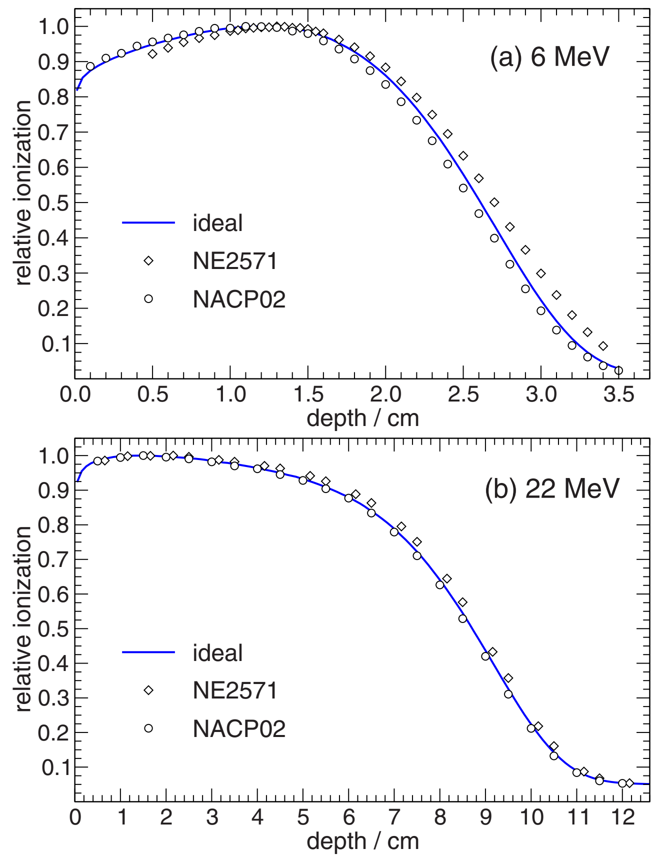

FIG. 1. Depth-ionization curves in a water phantom for an NACP02 plane-parallel chamber (circles) and an NE2571 Farmer-type chamber (diamonds) in (a) 6 MeV and (b) 22 MeV electron beams. The solid line is the ideal depth-ionization curve calculated by dividing the depth-dose curve by the water/air stopping-power ratio ($\Delta = 10$ keV) at the corresponding depth. All curves are normalized at d_{max}.

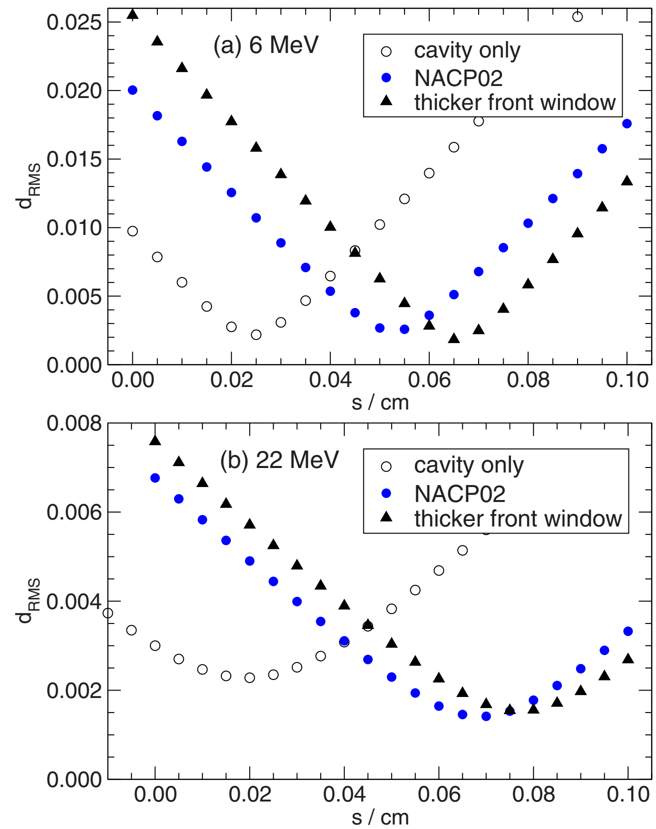

FIG. 2. Root-mean-square differences d_{rms} between two FDI curves [calculated by Eq. (4)] as a function of relative shift s between the two curves in (a) a 6 MeV and (b) a 22 MeV electron beam. A full NACP02 chamber (solid circles), an NACP02 chamber with 50% thicker front window (solid triangles), and a wall-less chamber (i.e., guarded air cavity only, open circles) are modeled.

$$d_{rms}(s) = \sqrt{\frac{\Sigma_i [p_s(z_i) - \alpha p_c(z_{0,i})]^2}{N}}, \tag{4}$$

where $p_s(z_i)$ and $p_c(z_{0,i})$ are the FDI values from the ideal and chamber FDI curves, respectively; $z_i = z_{0,i} + s$ is the shifted depth and $z_{0,i}$ is the original chamber depth at which p_c is calculated. The values of $p_s(z_i)$ are generally calculated by linear interpolations from two neighboring dose grid points. Only values of both $p_s(z_i)$ and $p_c(z_{0,i})$ greater than 0.05 are used in the calculation. The total number of points on the curves used in the calculation is N (>20 in this study). The value of d_{rms} can be thought of as the average fractional difference (normalized to the maximum ionization) between the two FDI curves. The effective point of measurement is obtained by finding the shift s that minimizes d_{rms}.

The chambers fully modeled in this study are an NACP02 chamber, a Markus chamber with or without a protection cap, and an NE2571 Farmer chamber (3.14 mm inner radius). The information for the plane-parallel chambers comes from the work of Mainegra-Hing *et al.*[16] The geometry and material information for these chambers can also be found in the IAEA's TRS-398.[4] For the NACP02 chamber, a calculation is done for a thicker front window (50% increase for both the Mylar and the graphite layer) since it is found experimentally that the front window of the NACP02 chamber may be thicker than specifications.[17] In addition to the full chamber models, the wall-less air cavities (with guard ring) of the NACP02 and the Markus chambers are also studied as are wall-less cylindrical air cavities of radii of 1, 3.14, and 5 mm. In principle, when wall and electrode effects are accounted for by the P_{wall} and P_{cel} corrections, the gradient correction (or EPOM) should correspond to values for the wall-less air cavities. However, in practice, these corrections were not made in experiments determining the EPOM and thus the calculations with the full chamber models are more appropriate in comparing to measurements.

II.B.1. Plane-parallel chambers

Figure 2 shows the minimized rms difference as a function of the relative shift for an NACP02 chamber, an NACP02 chamber with a thicker front window, and a wall-less NACP02 chamber cavity. The minimum rms difference occurs at a nonzero positive shift for both the real chamber and the wall-less cavity. For the wall-less cavity, the shift is about 0.2 mm for the two electron beams. The positive values of the shift suggest that there is a significant number of electrons scattered from the side walls and/or the cavity's distal face into the cavity, making the effective measuring

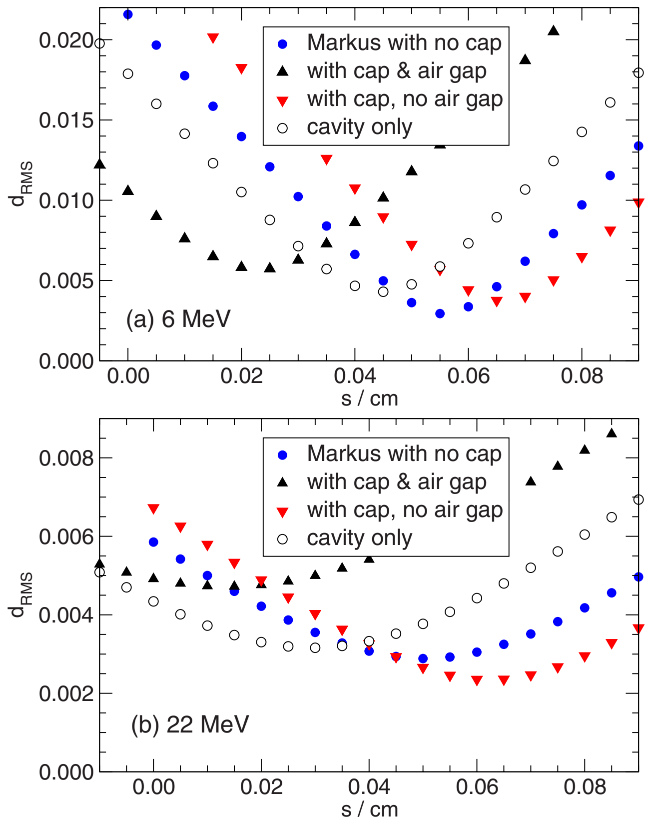

FIG. 3. Root-mean-square differences d_{rms} between two FDI curves [calculated by Eq. (4)] as a function of relative shift s between the two curves in (a) a 6 MeV and (b) a 22 MeV electron beam. A Markus chamber (solid circles), the air cavity of the chamber (open circles), the Markus chamber with a protective cap and an air gap (up triangles), and the chamber with a protective cap but no air gap (down triangles) are modeled.

point shift from the front face toward the center of the cavity. For the real chamber model, the shift is about 0.5–0.7 mm. The larger shift for the real model is because the chamber's front wall is mainly made of a layer of graphite of thickness of 0.5 mm, and, as the graphite density is 1.70 g/cm^3, it will make an extra 0.35 mm water equivalent material before the chamber cavity, compared to the wall-less cavity. The minimum rms difference (in percentage D_{max}) for the NACP02 chamber for the 22 MeV (6 MeV) beam is below 0.2% (0.3%) if the optimum effective point of measurement is taken into account, but it could be as large as 0.7% (2%) if the front face is taken as the effective point of measurement (i.e., no shift is used). For the chamber with the 50% thicker front window, the shift is a bit larger as expected. If no shift is used for the NACP02 chamber as is done in dosimetry protocols, the value of d_{rms} for a NACP02 chamber with a thicker front window is 2.5% for the 6 MeV beam, which is 25% larger than that (2%) for a NACP02 chamber with the specified front-window thickness.

A similar study was performed for the Markus chamber and results are shown in Fig. 3. As the entrance window is very thin for the Markus chamber, there is not much difference in the shift between the real chamber and the wall-less cavity (only 0.1–0.2 mm). For the wall-less cavity, it is seen that the minimum rms difference also occurs at a nonzero positive shift: 0.3 mm for the 22 MeV beam and 0.45 mm for the 6 MeV beam. The shifts are larger than those of the NACP02 chamber, especially for the low-energy beam. This is because the Markus chamber has a very narrow guard ring so that more electrons in the sensitive region are coming from the side wall. When the Markus chamber is used in a water phantom, a waterproof protective cap made of PMMA is needed. The protective cap has a thickness of 0.87 mm and there is an air gap of 0.4 mm between the cap and the chamber. Figure 3 also shows the influence of the protective cap, with or without the air gap, on the effective measuring point. When the protective cap is used, the entrance window thickness is dominated by the cap thickness. Since the PMMA has a density of 1.19 g/cm^3, when the cap is present but not the air gap, one would expect the shift to be $0.19\times 0.87=0.16$ mm larger than when no cap is used. This is exactly what Fig. 3 shows. If the air gap is present, it moves the effective measuring point back toward the front face of the cavity since there is lack of material before the cavity. Similar to the case of the NACP02 chamber, the Markus chamber would be less accurate if no shift is used. However, by using a protective cap with the air gap present, the accuracy is improved when no shift is used ($s=0$), although the minimum achievable rms difference becomes worse than when the effective point of measurement is shifted appropriately (i.e., $s>0$).

Another way to study the difference of the two FDI curves is to calculate the χ^2 values, similar to the method used by Kawrakow[18] in studying the effective point of measurement for cylindrical chambers in photon beams. The minimum χ^2 per degree of freedom for the NACP02 chamber in water in both the 6 and the 22 MeV beams is found to be 2.4 and 0.8, respectively, when the calculation uncertainty for the NACP02 FDI curves is about 0.2% (~0.8% at depths close to the practical range).

IAEA's TRS-398 recognizes the importance of the front-window issue, as it says "the water equivalent thickness (in g cm^{-2}) of the chamber wall and any waterproofing material should be taken into account when positioning the chamber at the point of interest. However, this is a very small effect and may be ignored in practice." So actually the front face of the cavity for plane-parallel chambers is still used as the effective point of measurement in the protocol. This presents a problem when comparing a depth-dose curve measured by a plane-parallel chamber to that by a cylindrical chamber as the effective point of measurement of a plane-parallel chamber may need to be shifted by roughly one-half a millimeter.

Table I shows the calculated shift needed in a water phantom in the 6 MeV electron beam for the guarded air cavities of a few plane-parallel chambers (i.e., the wall effect is excluded here). There is a correlation between the guard ring width and the calculated shift. The Attix chamber, which has a very large guard width, has a negligible shift. The relative shift between a Markus chamber cavity and a Roos chamber cavity is 0.27 mm, less than the experimental relative shift of 0.5 mm ($\sigma=0.2$ mm) found by Van der Plaetsen *et al.*[6] This is partly because the wall effect is excluded here. One may

TABLE I. The calculated relative shift in a 6 MeV electron beam for the guarded air cavities of several plane-parallel chambers (i.e., wall-less chambers) with different guard ring widths. The geometrical data for these chambers are from the IAEA's TRS-398 (Ref. 4).

	Markus	NACP	Roos	Exradin 11	Attix
Shift (mm)	0.45	0.25	0.18	0.13	0.02
Guard width (mm)	0.2	3	4	5.1	13.5
Collecting electrode diameter (mm)	5.3	10	16	20	12.7
Electrode spacing (mm)	2	2	2	2	1

conclude from this table that there are a significant number of electrons entering the cavity through side walls for those once believed "well-guarded" chambers, e.g., NACP02. For plane-parallel chambers the ratio of the collecting volume diameter to the electrode spacing is also an important parameter. It is recommended that this ratio be of the order of 10.[19] In Table I this ratio varies from 2.6 to 12.7 for these chambers, while the guard width varies from 0.2 to 13.5 mm. To separate the effect of diameter-to-spacing ratio from that of guard ring width, cavities having a fixed diameter-to-spacing ratio of 5 (as for NACP02 chamber) are simulated with different guard widths and the needed shifts are calculated. The results are listed in Table II. The shift obtained for the 10 mm guard width is comparable to that for the Exradin cavity of 5.1 mm guard width with a diameter-to-spacing ratio of 10 as shown in Table I. This demonstrates that, not only the 3 mm guard width of NACP02 chamber is too small but the diameter-to-spacing ratio of 5 is also too small for the chamber to be considered as well guarded.

II.B.2. Cylindrical chambers

Figure 4 shows the minimized rms difference as a function of the shift for the detailed model of the NE2571 chamber (wall and central electrode included) and for the cylindrical air cavities for both the 6 and 22 MeV beams. The shift is given as a fraction of the cavity radius r of the respective chambers. The negative value of the shift means it is upstream toward the radiation source, i.e., the ion chamber measures a dose closer to the radiation source. The difference between the results for the real NE2571 chamber (inner radius of 3.14 mm) and the air cavity of radius of 3.14 mm is due to the effects of the chamber wall and the central electrode, and it is small for high-energy electron beams. For the 22 MeV beam, the rms difference has a minimum value around a shift of $0.46r$ for the real NE2571 chamber and a shift of $0.51r$ for all the air cavities. This is almost the same as the value of $0.5r$ recommended by dosimetry protocols.[3,4]

TABLE II. The calculated relative shifts in a 6 MeV electron beam for several guarded air cavities with a fixed collecting volume diameter of 10 mm and a fixed electrode spacing of 2 mm for different guard ring widths.

	Cavity 1	Cavity 2 (NACP)	Cavity 3
Shift (mm)	0.39	0.25	0.11
Guard width (mm)	0.1	3	10

For the 6 MeV beam, the rms difference reaches a minimum at shifts of about $0.33r$ and $0.41r$ for the NE2571 realistic chamber model and all the air cavities, respectively. The values are less than recommended in dosimetry protocols. This difference is reasonable as the scattering effect is stronger for lower-energy beams so the effective point of measurement is closer to the center of the chamber. One more point from Fig. 4 is that the minimum rms difference for the high-energy beam (~0.4%) is smaller than in the low-energy beam (~1%), i.e., the cylindrical chamber is less appropriate for use in low-energy electron beams except for the very small radius cavity. If the $0.5r$ shift is also used for low-energy beams (e.g., 6 MeV), then the rms difference could be at least 2% for the NE2571 chamber, even though the minimum

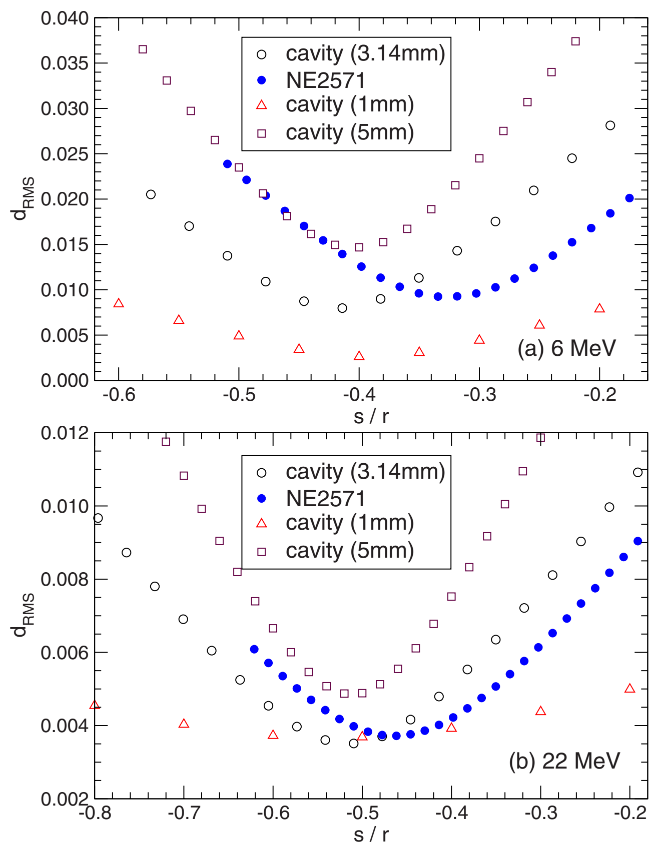

FIG. 4. Root-mean-square differences d_{rms} between two FDI curves [calculated by Eq. (4)] as a function of relative shift s between the two curves in (a) a 6 MeV and (b) a 22 MeV electron beam. A full model of NE2571 chamber (solid circles) and three cylindrical air cavities of different radii (1, 3.14, and 5 mm) are simulated. The shift is in units of the air cavity radius.

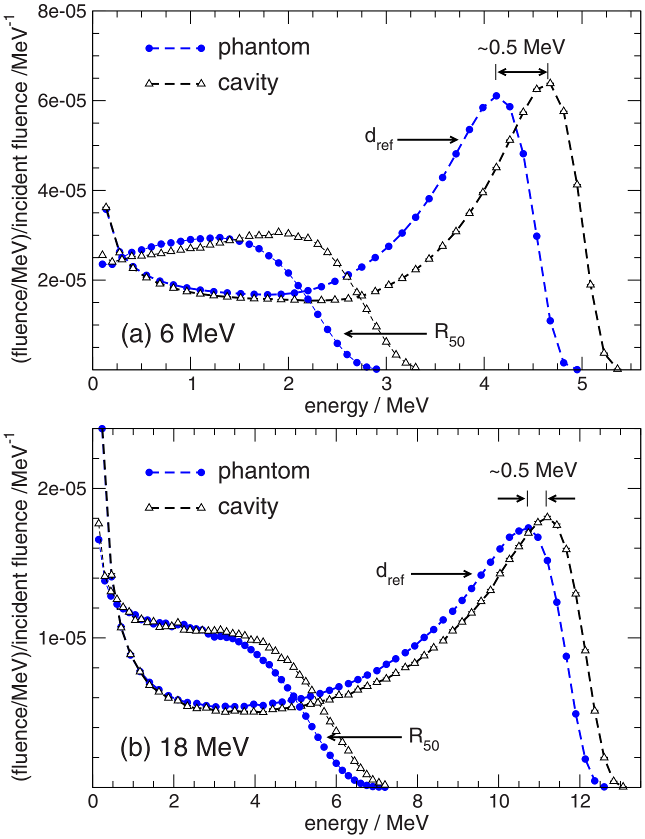

FIG. 5. Electron fluence spectra in a Farmer chamber cavity (open triangles) and in a water phantom (filled circles) at both d_{ref} and R_{50} in (a) a 6 MeV and (b) an 18 MeV electron beam.

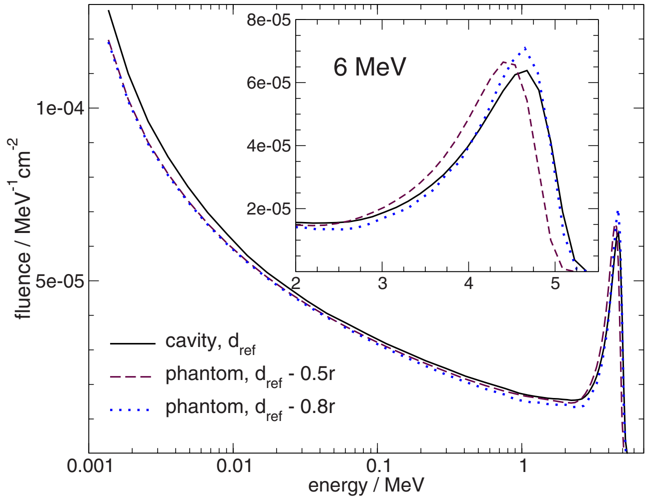

FIG. 6. Electron fluence spectra in the Farmer chamber cavity at d_{ref} (1.48 cm) and in the phantom at $d_{ref}-0.5r$ and $d_{ref}-0.8r$ in a 6 MeV electron beam. The inset shows, on a linear energy scale, the energy range near the peak of the primary electrons.

rms is 1%. The minimum χ^2 per degree of freedom for the NE2571 chamber in water in both the 6 and 22 MeV beams is found to be 67 and 7, respectively, when the calculation uncertainty for the NE2571 FDI curves is about 0.15% (~0.5% at depths close to the practical range). The very large χ^2 value for 6 MeV electron beam indicates again that with cylindrical chambers, a simple effective point of measurement correction is not enough to produce a reliable dosimeter, especially for low-energy electron beams.

II.C. Determining the EPOM from electron fluence spectra

As mentioned in Sec. I, the shape of the electron fluence spectrum (referred to as spectrum hereafter) in electron beams is continuously changing with depth. For cylindrical thimble chambers with the central axis at depth z (i.e., the point of measurement), there is a lack of phantom material upstream from the central axis of the chamber. It is expected that the spectrum in the chamber cavity is different from that at depth z in the phantom without the presence of the chamber. A detailed knowledge of the spectrum in the cavity and in the phantom is a useful way to study the perturbation effect of the cylindrical chamber cavity in electron beams. We used the CAVITY code with electron fluence calculation capability to calculate the spectrum in both the cavity and the phantom. Figure 5 shows the calculated spectra at d_{ref} and R_{50} in a water phantom and in a Farmer-type chamber cavity for both (a) a 6 MeV and (b) an 18 MeV electron beam. As expected, it is seen that the peak in the spectrum in the cavity is shifted to higher energy relative to that in the phantom. The energy shift is about 0.5 MeV and is not very sensitive to the depth or the electron beam energy. It is reasonable to believe that at a certain point in the phantom upstream from the point of measurement (z) in the phantom, the peak in the spectrum should match that in the cavity at the depth z. To find that point or the shift in distance s, the spectrum in the phantom is calculated for a variety of depths upstream from the depth z and compared to the spectrum in the cavity at the depth z. The shift in distance is found by matching the electron peaks in the spectrum. The shift found in this way for both a 3 mm radius (Farmer-type) chamber and a 5 mm radius chamber is $0.8r$, where r is the radius of the cylindrical cavity. This shift is different from the value obtained in Sec. II.B.2 or from the shift of $0.5r$ recommended by dosimetry protocols, since the mechanism of obtaining it is quite different: The current method only considers the peak of the electron fluence spectrum, which is essentially the peak of the primary electron fluence spectrum, while the previous method takes into account the whole PDD curve. However, it is very close to the theoretical value of $8r/3\pi \approx 0.85r$ calculated for cylindrical chambers in electron beams under the condition of no scattering as originally derived by Skaggs[20] and quoted by Nahum.[21]

Figures 6 and 7 show the spectra in the Farmer chamber cavity (3 mm radius) at d_{ref} compared to those at depths $d_{ref}-0.5r$ and $d_{ref}-0.8r$ in the phantom for the 6 and 18 MeV electron beams, respectively. It is seen that for the high-energy electron beam, the peak in the spectrum at $d_{ref}-0.8r$ in the phantom matches that in the cavity at d_{ref} excellently (Fig. 7 and the inset). For the low-energy electron beam the same shift also gives a match of the peaks in the spectrum, although the shape is not ideally matched (Fig. 6 and the

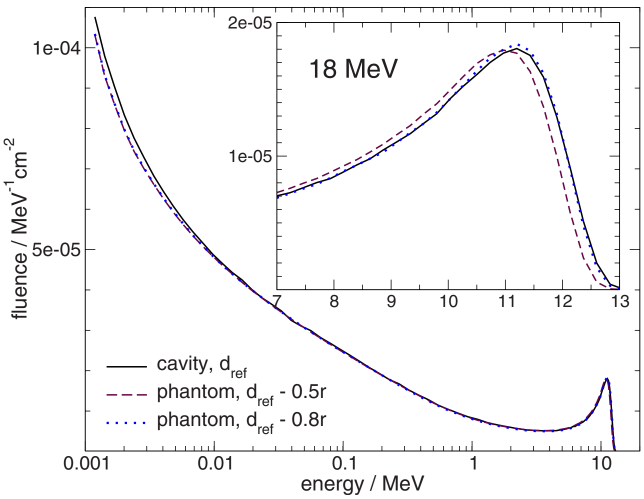

FIG. 7. Electron fluence spectra in the Farmer chamber cavity at d_{ref} (4.54 cm) and in the phantom at $d_{ref}-0.5r$ and $d_{ref}-0.8r$ in an 18 MeV electron beam. The inset shows, on a linear scale, the energy range near the peak of primary electrons.

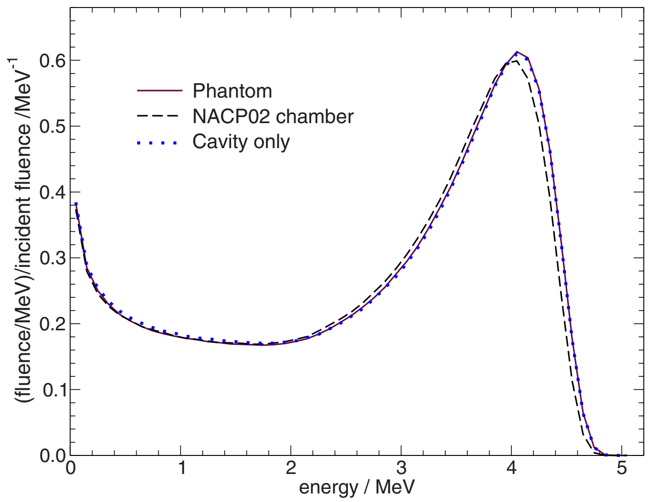

FIG. 8. Electron fluence spectrum in the phantom at d_{ref} in a 6 MeV electron beam compared to those in the NACP02 chamber and the wall-less chamber cavity with the front face of the cavity located at d_{ref}.

inset). There is a clear mismatch if the shift is $0.5r$ for both electron beams. The same results are obtained for the 5 mm radius cylindrical chamber. Experimentally, it is well known that cylindrical chambers are not recommended for use with low-energy electron beams since the fluence perturbation effect is large. It is interesting to note that the combination of the energy shift (0.5 MeV for Farmer chamber) and the distance shift ($0.8\times 0.3=0.24$ cm for Farmer chamber) studied above implies an electron stopping power of $0.5\ \mathrm{MeV}/0.24\ \mathrm{cm}\approx 2.1\ \mathrm{MeV/cm}$, which is consistent with the rule-of-thumb stopping power of 2 MeV/cm for high-energy electrons in water.

For plane-parallel chambers, as the front face of the cavity is the effective point of measurement, the match of the primary electron fluence spectra is mainly determined by the thickness of the chamber's front window. For a wall-less pancake shaped air cavity, one would expect the spectrum to be the same as that in the phantom. Figure 8 shows the comparison of the spectra in the phantom, in the NACP02 chamber, and in the wall-less NACP02 chamber cavity. The peak of the primary spectrum in the NACP02 chamber shifted to a lower energy compared to that in the phantom due to the extra 0.35 mm water-equivalent material before the cavity as estimated in Sec. II B. In determining the effective point of measurement for plane-parallel chambers by matching the electron fluence spectra, the wall effect should be separated out, i.e., we should match the spectra of the phantom and the wall-less cavity as done for cylindrical chambers. This leads to 0 shift according to Fig. 8, and this is what is currently used in dosimetry protocols.

Hence there are actually two ways of determining the effective point of measurement for ion chambers in electron beams: Either matching the primary electron fluence spectra or matching the depth-dose curves. Unfortunately, these two methods give different shifts for the effective point of measurement. If matching the depth-dose curves, for cylindrical chambers, the shift is in the range $0.4r$ to $0.5r$ upstream from the cavity center depending on the radiation quality but not on cavity radius; for plane-parallel chambers, the shift is in the range of 0.2–0.4 mm downstream from the cavity's front face depending on the radiation quality and the cavity geometry. If matching the primary electron fluence spectra, for cylindrical chambers, the shift is $0.8r$ upstream from the cavity center; for plane-parallel chambers, no shift is necessary.

III. THE ISSUE OF SELECTING THE STOPPING-POWER RATIO

From the results in Sec. II, for cylindrical chambers, since the electron fluence spectrum in the cavity at depth z is very different from that in the phantom at the same depth, the water/air stopping-power ratio cannot be simply evaluated at depth z in the phantom. Rather, the electron fluence spectrum in a cylindrical chamber cavity of radius r is similar to that in the phantom at a point $0.8r$ upstream from the chamber's central axis. Hence it is a reasonable approximation to assume that the water/air stopping-power ratio calculated for the electron fluence spectrum in the cavity is the same as that evaluated in phantom at depth $z-0.8r$. Figure 9 shows the calculated water/air stopping-power ratio as a function of depth for the 6 and 18 MeV electron beams. The gradients of the two lines are about 0.30%/mm and 0.16%/mm, respectively; this means that for a shift of $0.8r=2.4$ mm (i.e., for a Farmer chamber), the changes in the water/air stopping-power ratio are 0.72% and 0.38% for the 6 and 18 MeV beams, respectively.

As a way of verifying the applicability of the Spencer-Attix cavity theory as done previously,[2,22] the air in a Farmer chamber cavity is replaced by the low-density water (LDW) which has identical properties to liquid water except for the density. Since the density of LDW is the same as air, and since water and air have similar effective atomic number, the electron fluence spectrum in the LDW-filled cavity will be very close to that in the air-filled cavity. This is illustrated in

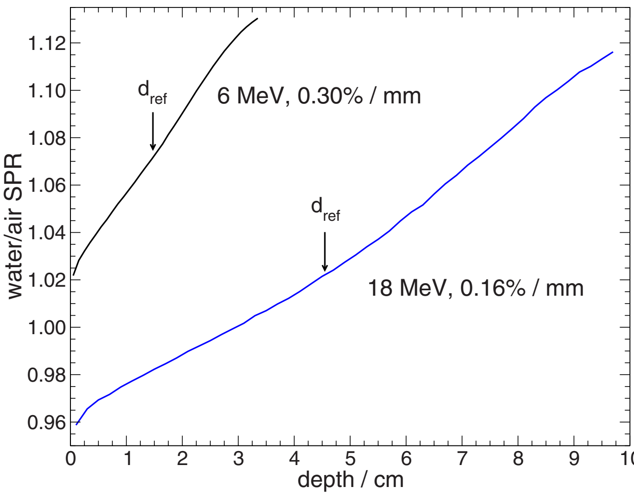

FIG. 9. The Spencer-Attix water/air stopping-power ratio (Δ=10 keV) vs depth for the 6 and 18 MeV electron beams.

Fig. 10, which shows the electron fluence spectra in the cavity filled with different gases at both d_{ref} and R_{50} in a 6 MeV electron beam. The spectra overlap each other for both depths at all energies above 10 keV. If the Farmer chamber cavity behaves like an ideal Spencer-Attix cavity (i.e., with no gradient or fluence corrections needed), then the ratios of the dose in the cavity filled with LDW to that in the cavity filled with air must be the same as the water/air stopping-power ratio evaluated at the point of measurement in the phantom. To investigate this, this cavity dose ratio is calculated at various depths in both the 6 and 18 MeV electron beams and the results are divided by the water/air stopping-power ratio (with Δ=10 keV) at the corresponding depths and at the depths shifted upstream by $0.5r$ and $0.8r$. The results are shown in Fig. 11. It is seen that, without the shift, the cavity dose ratio at d_{ref} deviates from the water/air stopping-power ratio by about 0.7% and 0.3% for the 6 and 18 MeV electron beams, respectively. This means that the

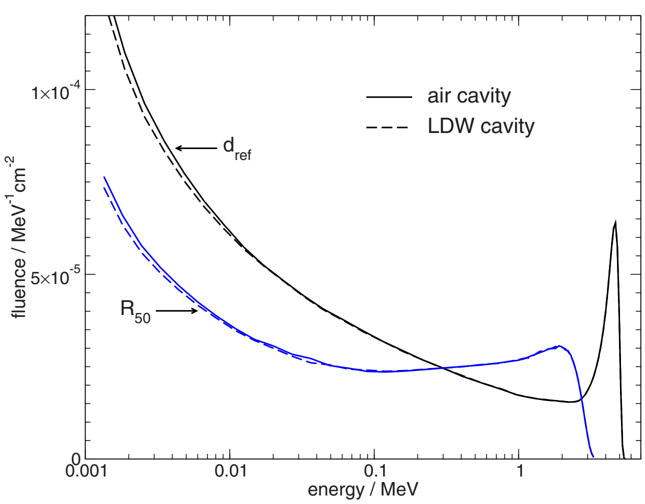

FIG. 10. Electron fluence spectra in the Farmer chamber cavity when the cavity is filled with either LDW or air at both d_{ref} and R_{50} in a 6 MeV electron beam.

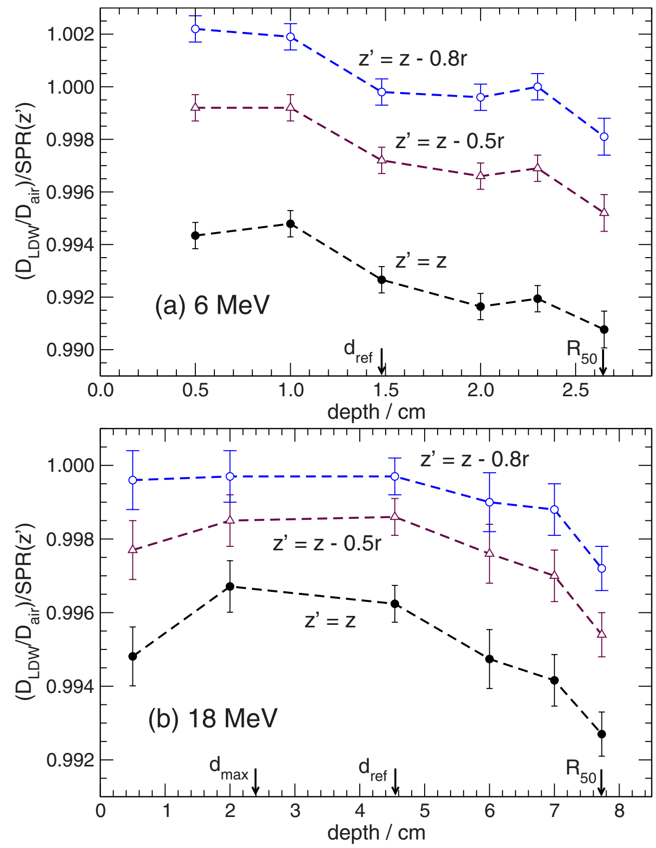

FIG. 11. The quotient of the dose ratio of the LDW cavity to air cavity for a Farmer chamber's cavity centered at z to the water/air stopping-power ratio (Δ=10 keV) evaluated at depths $z'=z$, $z-0.5r$, or $z-0.8r$ as a function of depth z in (a) a 6 MeV and (b) an 18 MeV electron beam.

cylindrical cavity deviates significantly from an ideal Spencer-Attix cavity. However, the cavity dose ratio is very close to the water/air stopping-power ratio evaluated at $z'=z-0.8r$ for both the electron beams especially at d_{ref}, which is consistent with the spectra looking similar (Figs. 6 and 7). A shift of $0.5r$, which is the dosimetry protocol recommendation, means the cavity dose ratio is closer to the stopping-power ratio than when no shift is used but not as close as when using a shift of $0.8r$ obtained by matching the primary electron fluence spectrum; there still remains a discrepancy of at least 0.2% at d_{ref} for a $0.5r$ shift in the 6 MeV beam.

In AAPM dosimetry protocols,[1,3] the point of measurement z is at the center of cylindrical chamber cavities and the water/air stopping-power ratio is also evaluated at this point. In TG-51,[3] a gradient correction factor, defined as the ratio of chamber reading at depth $z+0.5r$ to that at z, is explicitly used in the formula to account for the gradient effect. In the IAEA Code of Practice TRS-398,[4] the point of measurement z is called the reference point at which the water/air stopping-power ratio is evaluated and at which the dose is measured by shifting the cylindrical chamber downstream by an amount $s=0.5r$, i.e., at a depth $z+0.5r$. Thus the gradient effect is accounted for by the chamber shift. In both situations, the size of the shift, $s=0.5r$, is different from that determined by matching the shapes of the primary electron fluence spectra, $s=0.8r$. According to Fig. 11, this will lead to a systematic error in determining the dose at the reference depth z if the chamber is considered as a Spencer-Attix cavity. For plane-parallel chambers, there is no such problem when selecting the correct stopping-power ratio, since the shift is determined to be $s=0$ by matching the primary electron fluence spectra.

IV. CONCLUSIONS

Monte Carlo simulations by EGSnrc codes are employed to study the issue of effective point of measurement for both plane-parallel chambers and cylindrical thimble chambers in electron beams. The electron fluence spectra in phantom and in chamber cavities are studied. It is found that there are two ways of determining the position of the effective point of measurement: One is to match the calculated depth-ionization curve obtained from a modeled chamber or a wall-less chamber cavity to a calculated depth-dose curve; the other is to match the primary electron fluence spectrum in the wall-less chamber cavity to that in the phantom. For plane-parallel chambers, the effective point of measurement determined by the first method is generally not at the front face of the chamber cavity, which is what is obtained by matching the primary electron fluence spectrum, but shifted downstream toward the cavity center by 0.2–0.4 mm even for the wall-less cavities. The shift could be more than one-half a millimeter for a fully modeled plane-parallel chamber. This should not be ignored when measuring the depth-dose curves in electron beams using plane-parallel chambers. For cylindrical chambers, these two methods also give different positions of the effective point of measurement. Matching depth-ionization curves gives a shift of $0.5r$, which is in agreement with measurements for high-energy electron beams and is the same as the value currently used in major dosimetry protocols. Matching the electron spectra gives a shift of $0.8r$, which is closer to the value predicted by a theoretical calculation which assumes no-scatter conditions. The results show that the shift of $0.8r$ is more appropriate if the cylindrical chamber is to be considered as a Spencer-Attix cavity. As the water/air stopping-power ratio changes with depth in a water phantom in electron beams, the difference of the two shifts $(0.3r)$ for cylindrical chambers will lead to an incorrect evaluation of the water/air stopping-power ratio at the point of measurement in current dosimetry protocols. This results in a systematic error in determining the absorbed dose at the point. A reasonable approach is to use a shift of $0.8r$ for the electron beam source calibration since the stopping-power ratio is correctly evaluated and to use a shift of $0.4r$ or $0.5r$ (depending on the beam energy) for the percentage depth-dose curve measurements since it makes the average perturbation effect at all depths a minimum. For plane-parallel chambers, the front face of the air cavity can be taken as the effective point of measurement for electron beam calibration; however, for depth-dose measurements, the effective point of measurement may be shifted toward the cavity center by as much as one-half a millimeter.

ACKNOWLEDGMENTS

This work is supported by an Ontario Graduate Scholarship (OGS), NSERC, the Canada Research Chairs program, CFI, and OIT.

[a]Electronic mail: lwang@physics.carleton.ca
[b]Electronic mail: drogers@physics.carleton.ca

[1]AAPM TG-21, "A protocol for the determination of absorbed dose from high-energy photon and electron beams," Med. Phys. **10**, 741–771 (1983).
[2]L. L. W. Wang and D. W. O. Rogers, "Calculation of the replacement correction factors for ion chambers in megavoltage beams by Monte Carlo simulation," Med. Phys. **35**, 1747–1755 (2008).
[3]P. R. Almond, P. J. Biggs, B. M. Coursey, W. F. Hanson, M. S. Huq, R. Nath, and D. W. O. Rogers, "AAPM's TG–51 Protocol for Clinical Reference Dosimetry of High-Energy Photon and Electron Beams," Med. Phys. **26**, 1847–1870 (1999).
[4]IAEA, *Absorbed Dose Determination in External Beam Radiotherapy: An International Code of Practice for Dosimetry Based on Standards of Absorbed Dose to Water*, IAEA Technical Report Series (IAEA, Vienna, 2001), Vol. 398.
[5]K. A. Johansson, L. O. Mattsson, L. Lindborg, and H. Svensson, "Absorbed-dose determination with ionization chambers in electron and photon beams having energies between 1 and 50 MeV," in *IAEA Symposium Proceedings* (IAEA, Vienna, 1977), Paper No. IAEA-SM-222/35, pp. 243–270.
[6]IAEA, International Atomic Energy Agency Technical Report No. IAEA-TECDOC-1173, 2000.
[7]I. Kawrakow and D. W. O. Rogers, National Research Council of Canada Technical Report No. PIRS-701, 2000 (see http://www.irs.inms.nrc.ca/inms/irs/EGSnrc/EGSnrc.html).
[8]I. Kawrakow, "Accurate condensed history Monte Carlo simulation of electron transport. I. EGSnrc, the new EGS4 version," Med. Phys. **27**, 485–498 (2000).
[9]L. L. W. Wang and D. W. O. Rogers, "The replacement correction factors for cylindrical chambers in high-energy photon beams," Phys. Med. Biol. **54**, 1609–1620 (2009).
[10]L. L. W. Wang and D. W. O. Rogers, "The replacement correction factors for cylindrical chambers in electron beams," Med. Phys. (submitted).
[11]D. W. O. Rogers, I. Kawrakow, J. P. Seuntjens, and B. R. B. Walters, National Research Council Technical Report No. PIRS-702, 2000.
[12]I. Kawrakow, National Research Council of Canada Technical Report No. PIRS-899, 2005.
[13]D. W. O. Rogers, B. A. Faddegon, G. X. Ding, C.-M. Ma, J. Wei, and T. R. Mackie, "BEAM: A Monte Carlo code to simulate radiotherapy treatment units," Med. Phys. **22**, 503–524 (1995).
[14]F. H. Attix, *Introduction to Radiological Physics and Radiation Dosimetry* (Wiley, New York, 1986).
[15]L. V. Spencer and F. H. Attix, "A theory of cavity ionization," Radiat. Res. **3**, 239–254 (1955).
[16]E. Mainegra-Hing, I. Kawrakow, and D. W. O. Rogers, "Calculations for plane-parallel ion chambers in ^{60}Co beams using the EGSnrc Monte Carlo code," Med. Phys. **30**, 179–189 (2003).
[17]E. Chin, D. Shipley, M. Bailey, J. Seuntjens, H. Palmans, A. DuSautoy, and F. Verhaegen, "Validation of a Monte Carlo model of a NACP-02 plane-parallel ionization chamber model using electron backscatter experiments," Phys. Med. Biol. **53**, N119–N126 (2008).
[18]I. Kawrakow, "On the effective point of measurement in megavoltage photon beams," Med. Phys. **33**, 1829–1839 (2006).
[19]IAEA, International Atomic Energy Agency Technical Report Series No. 381, 1997.
[20]L. S. Skaggs, "Depth dose of electrons from the betatron," Radiology **53**, 868–873 (1949).
[21]A. E. Nahum, "Perturbation effects in dosimetry: Part I. Kilovoltage x-rays and electrons," Phys. Med. Biol. **41**, 1531–1580 (1996).
[22]L. L. W. Wang, D. J. La Russa, and D. W. O. Rogers, "Systematic uncertainties in the Monte Carlo calculation of ion chamber replacement correction factors," Med. Phys. **36**, 1785–1789 (2009).